On the Total Variation of High-Order Semi-Discrete Central Schemes for Conservation Laws

Steve Bryson* Doron Levy†

October 18, 2004

Abstract

We discuss a new fifth-order, semi-discrete, central-upwind scheme for solving one-dimensional systems of conservation laws. This scheme combines a fifth-order WENO reconstruction, a semi-discrete central-upwind numerical flux, and a strong stability preserving Runge-Kutta method. We test our method with various examples, and give particular attention to the evolution of the total variation of the approximations.

Key words. high-order, central schemes, conservation laws, total variation.

AMS(MOS) subject classification. 65M06.

1 Introduction

In this paper we present a fifth-order, essentially non-oscillatory central-upwind scheme that is designed to solve systems of conservation laws of the form

$$q_t + f(q)_x = 0. \tag{1.1}$$

Here $q \in \mathbb{R}^p$ is a p-dimensional solution vector and f is a p-dimensional flux function. The solution of (1.1) may become singular in finite time, which in turn requires a careful study when dealing with numerical approximations.

*NASA Advanced Supercomputing Division, NASA Ames Research Center, Moffett Field, CA 94035-1000; bryson@nas.nasa.gov

†Department of Mathematics, Stanford. University, Stanford, CA 94305-2125; dlevy@math.stanford.edu

One approach to approximating solutions of (1.1) is to use high-order, non-oscillatory central methods, which were introduced in [14]. Central methods avoid approximating the solution of (1.1) at singularities of the solution, and so do not require solving Riemann problems. The resulting simplicity makes central schemes well-suited for systems and multiple dimensions. Central-upwind schemes, introduced in [7] and refined in [5], are semi-discrete variants of central methods which have improved efficiency and less dissipation than fully-discrete central methods. Our work uses the numerical flux of [5], which we refer to as the KNP flux.

In this work we combine the KNP flux with the fifth-order weighted essentially non-oscillatory (WENO) reconstruction of [3], and the five-stage fourth-order strong stability preserving (SSP) Runge-Kutta method of [17], which is based on [1]. This is the first time these particular ingredients are combined into one scheme.

Fourth-order fully-discrete central schemes based on WENO reconstructions were presented in [9, 12]. The total variation behavior of these methods was examined in [11], where numerical experiments indicate that though the WENO-based methods are not total variation diminishing (TVD), they are total variation bounded. Fifth- and ninth-order fully-discrete central schemes are discussed in [15]. Third-order extensions of the KNP scheme can be found in [4, 6].

In this paper we investigate the evolution in time of the total variation (TV) of our scheme. The total variation is defined for a discrete solution u_j as $\mathrm{TV}(u) := \sum_j |u_{j+1} - u_j|$. In the case of systems TV is defined as the sum of the TV over the components. A scheme is called TV bounded (TVB) in $0 \le t \le T$ if $\mathrm{TV}(u) \le K$ for fixed $K > 0$ which depends only on initial conditions, and $\forall n$ and Δt such that $n\Delta t \le T$. In the scalar case, if a scheme is TVB then there exists a convergent subsequence in L^1_{loc} to a weak solution of (1.1), which turns into strong convergence if an additional entropy condition is satisfied (see [8]). Our numerical experiments indicate that our method is TVB, providing evidence of the convergence of the method.

The structure of this paper is as follows: In Section 2 we present our fifth-order central-upwind scheme, summarizing the derivation of the KNP flux in Section 2.1. The WENO reconstruction is presented in Section 2.2 and the fourth-order SSP-RK method in Section 2.3. Section 3 presents the results of a number of numerical tests of our method. We test both the accuracy and the evolution of the total variation of the resulting approximations.

Acknowledgment: The work of D. Levy was supported in part by the National Science Foundation under Career Grant No. DMS-0133511.

2 The Numerical Scheme

We briefly summarize the components we use to construct our fifth-order central-upwind scheme; the numerical flux from [5], the reconstruction from [3] and the ODE solver from [17]. This is the first time these particular ingredients are combined into one scheme.

2.1 The KNP Flux

Throughout this section we assume a one-dimensional grid $\{x_j\}$ with constant spacing Δx. We define $x_{j\pm\frac{1}{2}} := x_j \pm \frac{1}{2}\Delta x$ and the cell $I_j = \left[x_{j-\frac{1}{2}}, x_{j+\frac{1}{2}}\right]$. For any function $f(x)$ we use the notation $f_j := f(x_j)$. The cell average of q in the cell I_j is given by $\bar{q}_j := \frac{1}{\Delta x}\int_{x_{j-\frac{1}{2}}}^{x_{j+\frac{1}{2}}} q(x)\,dx$.

We assume that the cell-averages $\bar{q}_j^n$ are known at time t^n. The first step in the derivation of the approximate solution is to generate a piecewise-polynomial reconstruction from these cell-averages. Such a global reconstruction is defined as $\tilde{q}(x) = \sum_j \tilde{q}_j(x)\chi_{I_j}(x)$, where $\chi_{I_j}(x)$ is the characteristic function of I_j, and $\tilde{q}_j(x)$ are polynomials of a suitable degree.

In each cell I_j the reconstruction $\tilde{q}_j(x)$ should be conservative, *i.e.* $\frac{1}{\Delta x}\int_{x_{j-\frac{1}{2}}}^{x_{j+\frac{1}{2}}} \tilde{q}_j(x)\,dx = \bar{q}_j$, sth-order accurate, so $\tilde{q}_j(x) = q(x) + O(\Delta x^s)$ for $x \in I_j$, and non-oscillatory. Given such a reconstruction, we denote the point-values of $\tilde{q}$ at the interfaces of the cell I_j by $q^+_{j+\frac{1}{2}} := \tilde{q}_{j+1}\left(x_{j+\frac{1}{2}}\right)$ and $q^-_{j+\frac{1}{2}} := \tilde{q}_j\left(x_{j+\frac{1}{2}}\right)$.

The local speeds of propagation of information from the discontinuities at the cell interfaces, $a_{j\pm\frac{1}{2}}$, are given by

$$a^+_{j+\frac{1}{2}} = \max\left(\lambda_j\left(\frac{\partial f}{\partial q}\right), 0\right), \quad a^-_{j+\frac{1}{2}} = \left|\min\left(\lambda_j\left(\frac{\partial f}{\partial q}\right), 0\right)\right|.$$

Here, $\lambda_j\left(\frac{\partial f}{\partial q}\right)$ denote the eigenvalues of the Jacobian of f evaluated at $x_{j+\frac{1}{2}}$. These local speeds of propagation are then used to determine evolution points that are away from the propagating discontinuities. An exact evolution of the reconstruction at these evolution points is followed by an intermediate piecewise polynomial reconstruction and finally projected back onto the original cells, providing the cell-averages at the next time-step $\bar{q}_j^{n+1}$. Further details can be found in [5]. A semi-discrete scheme is obtained in the limit as $\Delta t \to 0$, yielding the KNP central-upwind scheme

$$\frac{d\bar{q}_j}{dt} = -\frac{H_{j+\frac{1}{2}} - H_{j-\frac{1}{2}}}{x_{j+\frac{1}{2}} - x_{j-\frac{1}{2}}}. \tag{2.1}$$

The numerical flux in (2.1) is given by

$$H_{j+\frac{1}{2}} = \frac{a^+_{j+\frac{1}{2}} f\left(q^-_{j+\frac{1}{2}}\right) + a^-_{j+\frac{1}{2}} f\left(q^+_{j+\frac{1}{2}}\right)}{a^+_{j+\frac{1}{2}} + a^-_{j+\frac{1}{2}}} - \frac{a^+_{j+\frac{1}{2}} a^-_{j+\frac{1}{2}}}{a^+_{j+\frac{1}{2}} + a^-_{j+\frac{1}{2}}} \left[q^+_{j+\frac{1}{2}} - q^-_{j+\frac{1}{2}}\right].$$

The accuracy of this scheme is determined by the accuracy of the reconstructions and the ODE solver.

It is straightforward to generalize this scheme to higher dimensions, using dimension-by-dimension reconstructions. Care must be taken, however, to use higher-order quadratures in the derivation of the KNP flux in higher dimensions to maintain accuracy. See [6] for a third-order example.

2.2 The Fifth-Order WENO Reconstruction

Weighted, essentially non-oscillatory (WENO) reconstructions [3, 13] are based on the essentially non-oscillatory (ENO) reconstructions of [2, 16]. ENO schemes choose the stencil that provide the least oscillatory reconstruction. WENO schemes weight all stencils so that accuracy is gained in smooth regions while avoiding crossing discontinuities.

We use the fifth-order WENO reconstruction of the point-value $q_{j+\frac{1}{2}}$ given in [3]. We begin with the three quadratic reconstructions on three-point stencils

$$q^k_{j+\frac{1}{2}} = \sum_{r=0}^{2} a^k_r \bar{q}_{j+k+r-2}, \tag{2.2}$$

where k ranges from 0 to 2 and the coefficients a^k_r, given in Table 2.1, are defined so that (2.2) approximates $q\left(x_{j+\frac{1}{2}}\right)$ with third-order accuracy. The WENO reconstruction is then defined as the convex combination

$$q_{j+\frac{1}{2}} = \sum_{k=0}^{2} w^k_j q^k_{j+\frac{1}{2}}, \qquad w^k_j := \frac{\alpha^k_j}{\sum_{k=0}^{2} \alpha^k_j}, \qquad \alpha^k_j := \frac{C^k}{\left(\epsilon + S^k_j\right)^2}. \tag{2.3}$$

The constants $C^k = \{1/10, 6/10, 3/10\}$ are defined so that $\sum_{k=0}^{2} C^k q^k_{j+\frac{1}{2}}$ approximates $q\left(x_{j+\frac{1}{2}}\right)$ with fifth-order accuracy. S^k_j is a smoothness measure which is large when $q^k_{j+\frac{1}{2}}$ has large variation. S^k_j approximates the L_2-norm of the first two derivatives of q, and is given by

$$\begin{aligned}
S^0_j &= \frac{13}{12}\left(\bar{q}_{j-2} - 2\bar{q}_{j-1} + \bar{q}_j\right)^2 + \frac{1}{4}\left(\bar{q}_{j-2} - 4\bar{q}_{j-1} + 3\bar{q}_j\right)^2 \\
S^1_j &= \frac{13}{12}\left(\bar{q}_{j-1} - 2\bar{q}_j + \bar{q}_{j+1}\right)^2 + \frac{1}{4}\left(\bar{q}_{j-1} - \bar{q}_{j+1}\right)^2 \\
S^2_j &= \frac{13}{12}\left(\bar{q}_j - 2\bar{q}_{j+1} + \bar{q}_{j+2}\right)^2 + \frac{1}{4}\left(3\bar{q}_j - 4\bar{q}_{j+1} + \bar{q}_{j+2}\right)^2.
\end{aligned} \tag{2.4}$$

Following [3] we take $\epsilon = 10^{-6}$. The reconstruction of $q_{j-\frac{1}{2}}$ on the stencil centered at x_j is obtained by symmetry. For more details consult [3].

k	$r=0$	$r=1$	$r=2$
0	1/3	-7/6	11/6
1	-1/6	5/6	1/3
2	1/3	5/6	-1/6

Table 2.1: Coefficients a_r^k for the quadratic reconstructions (2.2).

2.3 The Fourth-Order SSP Runge-Kutta ODE Solver

We use an optimal, strong stability preserving fourth-order accurate five-stage Runge-Kutta solver from [17]. We write this method as an explicit 5-stage Runge-Kutta solver for the ODE $dq/dt = F(q)$ as

$$\begin{aligned} q^{(0)} &= q^n, \\ q^{(s)} &= \sum_{i=0}^{s-1} \left(\alpha_{si} q^{(i)} + \Delta t \beta_{si} F\left(q^{(i)}\right) \right), \\ q^{n+1} &= q^{(4)}, \end{aligned} \tag{2.5}$$

where $s = 0, \ldots, 4$ and

$$\begin{aligned} &\alpha_{0,0} = 1.0, \quad \alpha_{1,0} = 0.44437049406734, \quad \alpha_{1,1} = 0.55562950593266, \\ &\alpha_{2,0} = 0.62010185138540, \quad \alpha_{2,1} = 0, \quad \alpha_{2,2} = 0.37989814861460, \\ &\alpha_{3,0} = 0.62010185138540, \quad \alpha_{3,1} = \alpha_{3,2} = 0, \quad \alpha_{3,3} = 0.82192004589227, \\ &\alpha_{4,0} = 0.00683325884039, \quad \alpha_{4,1} = 0, \quad \alpha_{4,2} = 0.51723167208978, \\ &\alpha_{4,3} = 0.12759831133288, \quad \alpha_{4,4} = 0.34833675773694, \\ &\beta_{0,0} = 0.39175222700392, \\ &\beta_{1,0} = 0, \qquad \beta_{1,1} = 0.36841059262959, \\ &\beta_{2,0} = \beta_{2,1} = 0, \qquad \beta_{2,2} = 0.25189177424738, \\ &\beta_{3,0} = \beta_{3,1} = \beta_{3,2} = 0, \qquad \beta_{3,3} = 0.54497475021237, \\ &\beta_{4,0} = \beta_{4,1} = \beta_{4,2} = 0, \qquad \beta_{4,3} = 0.08460416338212, \\ &\beta_{4,3} = 0.22600748319395. \end{aligned}$$

In our examples we use the CFL condition $\Delta t = 0.9 \min_j \frac{\Delta x}{|\lambda_j|}$, where here λ_j denote the eigenvalues of the Jacobian of f evaluated at x_j.

3 Numerical Examples

We test our method on various examples, measuring both the accuracy and the evolution of the TV over time. When an exact solution is not available, we use a high-resolution reference solution computed using the second order KNP method as presented in [5], which is known to be TVD. Unless otherwise stated, this reference solution uses $N = 5000$ nodes.

We first test our method with the scalar advection problem $u_t + u_x = 0$, $u(x, t = 0) = \sin^4(\pi x)$ on the periodic domain $[-1, 1]$ to $T = 2$. The relative L^1- and L^∞- norms of the errors are shown in Table 3.1. We also test accuracy with the Burgers equation $u_t + \left(\frac{u^2}{2}\right)_x = 0$, $u(x, t = 0) = 3 + \sin(x)$ on the periodic domain $[0, 1\pi]$ at $T = 0.5$, before shock formation, and at $T = 2.5$ after shock formation. The results are also shown in Table 3.1. Figure 3.1 shows the result at $T = 2.5$, as well as the change in TV over time for various resolutions. For this example the exact TV equals to 4 before the singularity formation at $T = 1$.

N	*relative* L^1*-error*	L^1*-order*	*relative* L^∞*-error*	L^∞-order
	Linear Advection of $\sin^4(\pi x)$, $T = 2$			
100	8.56×10^{-4}	-	2.73×10^{-5}	-
200	2.58×10^{-5}	5.05	5.53×10^{-7}	5.62
400	6.68×10^{-7}	5.27	7.05×10^{-9}	6.30
800	1.90×10^{-8}	5.14	6.84×10^{-11}	6.69
	Burgers equation before the shock, $T = 0.5$			
100	1.09×10^{-6}	-	1.08×10^{-7}	-
200	4.30×10^{-8}	4.66	1.94×10^{-9}	5.80
400	1.46×10^{-9}	4.88	3.62×10^{-11}	5.74
800	1.07×10^{-10}	3.78	8.38×10^{-13}	5.43
	Burgers equation after the shock, $T = 2.5$			
100	3.13×10^{-3}	-	1.74×10^{-3}	-
200	1.93×10^{-3}	0.70	1.40×10^{-3}	0.31
400	7.95×10^{-4}	1.28	4.98×10^{-4}	1.49
800	4.16×10^{-4}	0.93	2.61×10^{-4}	0.93

Table 3.1: Relative L^1 and L^∞ errors for the advection equation and the Burgers equation

Our next example is Burgers equation on the same domain with initial data $u(x, t = 0) = 2 - \sin(x) + \sin(2x)$. This example develops two shocks which eventually merge. Figure 3.2 shows the solution at $T = 1.2$ as well as the change in TV over time for various resolutions.

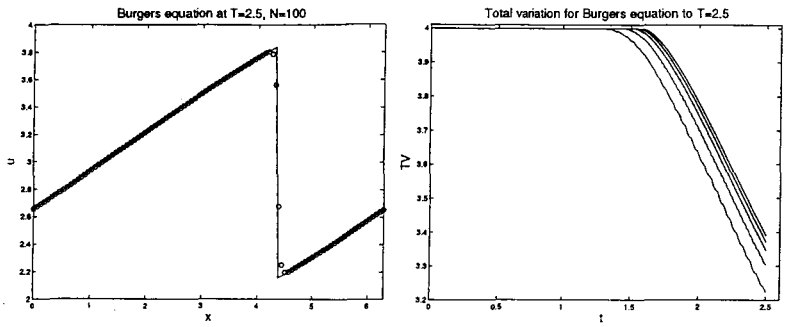

Figure 3.1: Results for the Burgers equation using the central-upwind scheme (2.1), (2.3) and (2.5). *Left:* the solution after shock formation at $T = 2.5$, "$-$": exact solution, "o": approximation. *Right:* the change in the TV of the approximation for $N = 100, 200, 400, 800$ nodes (from left to right) compared with the TV of a reference solution (the upper curve).

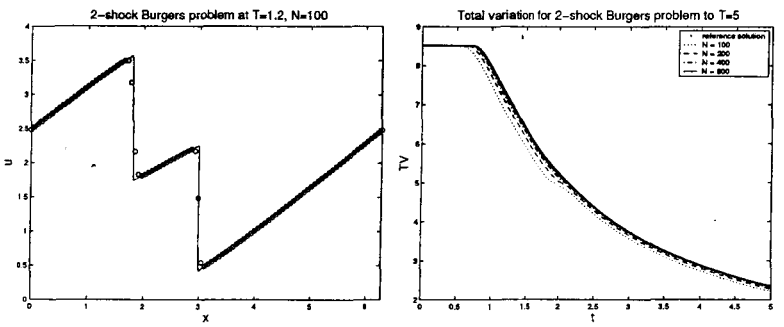

Figure 3.2: Results for Burgers equation with initial data that develops a double shock using the central-upwind scheme (2.1), (2.3) and (2.5). *Left:* the solution after shock formation at $T = 1.2$, "$-$": exact solution, "o": approximation. *Right:* the change in the TV of the approximation for various resolutions compared with the TV of a reference solution.

Turning to systems, we consider the Euler equations

$$\begin{pmatrix} \rho \\ \rho u \\ E \end{pmatrix}_t + \begin{pmatrix} \rho u \\ \rho u^2 + p \\ (E+p)\,u \end{pmatrix}_x = 0, \tag{3.1}$$

with equation of state $p = (\gamma - 1)\left(E - \frac{1}{2}\rho u^2\right)$ and $\gamma = 1.4$. We first apply our method to the Sod problem on the domain $[0, 1]$ with initial data

$$(\rho, u, E) = \begin{cases} (1.0, 0.0, 2.5), & x < 0.5, \\ (0.125, 0.0, 0.25), & x > 0.5. \end{cases} \tag{3.2}$$

The results at $T = 0.16$ with $N = 100$ grid nodes is shown in Figure 3.3 where we see that the shocks and the contact discontinuity are well captured by this scheme even at this low resolution. Figure 3.3 also shows the TV behavior of the approximation, compared with a reference solution. We see that the TV of the approximate solutions is greater than that of the reference solution, but damps with time suggesting that the approximations are TV bounded.

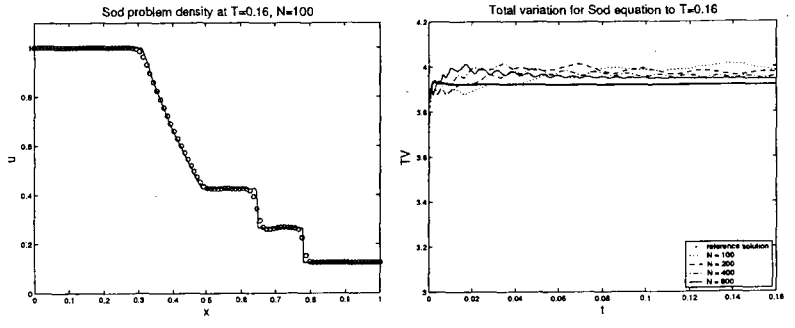

Figure 3.3: Results for the Sod problem (3.2) using the central-upwind scheme (2.1), (2.3) and (2.5). *Left:* Density. "–": reference solution, "o": approximation with $N = 100$ nodes. *Right:* the change in the TV of the approximation for various resolutions compared with the TV of a reference solution.

We now apply our method to the Lax problem on the domain $[0, 1]$ with initial data

$$(\rho, u, E) = \begin{cases} (0.445, 0.311, 8.928), & x < 0.5, \\ (0.5, 0.0, 1.4275), & x > 0.5. \end{cases} \tag{3.3}$$

The results at $T = 0.16$ with $N = 100$ and $N = 400$ grid nodes is shown in Figure 3.4. While the shock and the contact discontinuity are well-captured

at low resolution, there is significant oscillation between the contact discontinuity and the shock for $N = 100$. Figure 3.4 also shows the TV behavior of the approximation, compared with a reference solution. Similarly to the Sod problem, we see that the TV of the approximate solutions is initially greater than that of the reference solution, but converges to the TV of the reference solution.

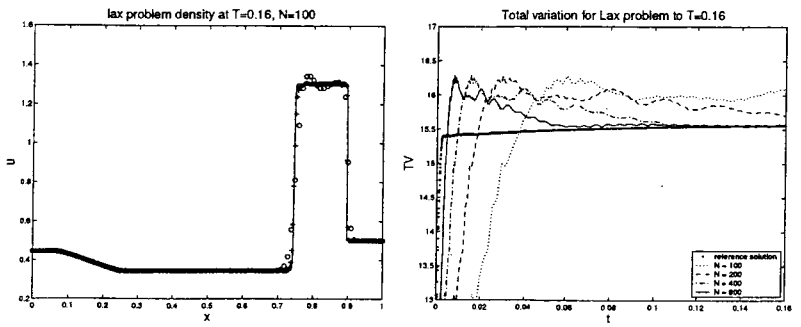

Figure 3.4: Results for the Lax problem (3.3) using the central-upwind scheme (2.1), (2.3) and (2.5). *Left:* Density. "−": reference solution, "o": approximation with $N = 100$ nodes, "+": approximation with $N = 400$ nodes. *Right:* the change in the TV of the approximation for various resolutions compared with the TV of a reference solution.

For our final example we apply our method to the problem of a mach 3 wave interacting with an acoustic shock on the domain $[0, 1]$, see [16]. The initial conditions for this problem are

$$(\rho, u, p) = \begin{cases} (3.857143, 2.629369, 10.3333), & x \leq 0.1, \\ (1 + 0.2\sin(50x), 0, 1), & x > 0.1. \end{cases} \tag{3.4}$$

The results are shown in Figure 3.5, compared with a reference solution using 20,000 nodes. We see the high resolution of our method and indications that the TV of our approximations converges to that of the reference solution.

References

[1] Gottlieb, S., Shu, C.-W., Tadmor, E., *Strong stability-preserving high order time discretization methods*, SIAM Review, **43** (2001), pp.89–112.

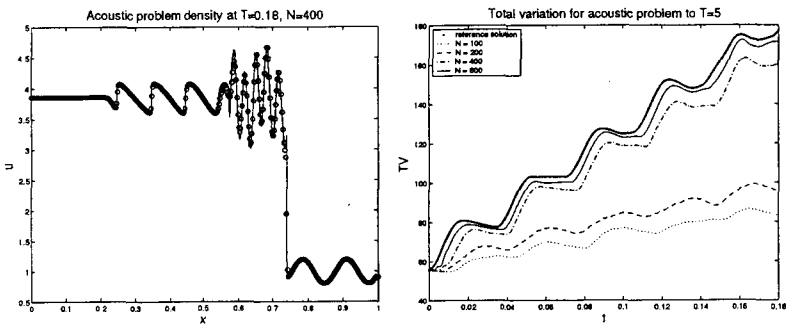

Figure 3.5: Results for the acoustic-shock problem (3.4), showing the approximation of the density field at $T = 0.18$ using $N = 400$ nodes. *Left:* Approximate solution. "–": reference solution, "o": approximation. *Right:* the change in the TV of the approximation for various resolutions compared with the TV of a reference solution.

[2] Harten, A., Engquist, B., Osher, S., Chakravarthy, S., *Uniformly high order accurate essentially non-oscillatory schemes III*, J. Comp. Phys., **71** (1987), pp.231–303.

[3] Jiang, G.-S., Shu, C.-W., *Efficient implementation of weighted ENO schemes*, J. Comp. Phys., **126** (1996), pp.202–228.

[4] Kurganov, K., Levy, D., *A Third-order semi-discrete central scheme for conservation laws and convection-diffusion equations* , SIAM J. Sci. Comp., **22** (2000), pp.1461–1488.

[5] Kurganov, K., Noelle, S., Petrova, G., *Semi-discrete central-upwind schemes for hyperbolic conservation laws and Hamilton-Jacobi equations* , SIAM J. Sci. Comp., **23** (2001), pp.707–740.

[6] Kurganov, K., Petrova, G., *A Third-order semi-discrete genuinely multidimensional central scheme for hyperbolic conservation laws and related problems* , Numer. Math., **88** (2001), pp.683–729.

[7] Kurganov, A., Tadmor, E., *New high-resolution central schemes for nonlinear conservation laws and convection-diffusion equations*, J. Comp. Phys., **160** (2000), pp.241–282.

[8] LeVeque, R. J., *Numerical Methods for Conservation Laws*, Lectures in Mathematics, Birkhuser, Basel,1992.

[9] Levy, D., Puppo, G., Russo, G., *Central WENO schemes for hyperbolic systems of conservation laws*, Math. Model. and Numer. Anal., **33** (1999), pp.547–571.

[10] Levy, D., Puppo, G., Russo, G., *Compact central WENO schemes for multidimensional conservation laws*, SIAM J. Sci. Comp., **22** (2000), pp.656–672.

[11] Levy, D., Puppo, G., Russo, G., *On the behavior of the total variation in CWENO methods for conservation laws*, Appl. Num. Math., **33** (2000), pp.415–421.

[12] Levy, D., Puppo, G., Russo, G., *A fourth order central WENO scheme for multi-dimensional hyperbolic systems of conservation laws* , SIAM J. Sci. Comp., **24** (2002), pp.480–506.

[13] Liu, X.-D., Osher, S., Chan, T., *Weighted essentially non-oscillatory schemes*, J. Comp. Phys., **115** (1994), pp.200–212.

[14] Nessyahu, H., Tadmor, E., *Non-oscillatory central differencing for hyperbolic conservation laws*, J. Comp. Phys., **87** (1990), pp.408–463.

[15] Qiu, J., Shu, C.-W., *On the construction, comparison, and local characteristic decomposition for high order central WENO schemes*, J. Comp. Phys., **183** (2002), pp.187–209.

[16] Shu, C.-W., Osher, S., *Efficient implementation of essentially non-oscillatory shock-capturing schemes*, J. Comp. Phys., **77** (1988), pp.439–471.

[17] Spiteri, R. J., Ruuth, S. J., *A new class of optimal high-order strong-stability-preserving time discretization methods*, SIAM J. Numer. Anal., **40** (2002), pp.469–491.